RSC Advances

ROYAL SOCIETY OF CHEMISTRY

www.rsc.org/advances

Zero-Valent Iron Nanoparticle with Sustained High Reductive Activity for Carbon Tetrachloride Dechlorination

Ying-Chao Huo [1,2], Wen-Wei Li [2,*], Di Min [2], Dan-Dan Wang [1], Hou-Qi Liu [1], Qin Kong [1], Tai-Chu Lau [1,3], Raymond J. Zeng [1,2,**]

[1] Advanced Laboratory for Environmental Research & Technology (ALERT), USTC-CityU, Suzhou 215123, China

[2] CAS for Unban Pollutant Conversion, Department of Chemistry, University of Science and Technology of China, Hefei 230026, China

[3] Department of Biology and Chemistry, City University of Hong Kong, Tat Chee Avenue, Kowloon, Hong Kong SAR, Hong Kong

Corresponding Authors:

*Corresponding author. Tel.: (+86)51287161361; Fax: (+86)51287161381. E-mail address: wwli@ustc.edu.cn (Wen-Wei Li)

** Corresponding author. Tel.: (+86)55163600203; Fax: (+86)55163601592. E-mail address: rzeng@ustc.edu.cn (Raymond J. Zeng).

Abstract

Zero-Valent Iron nanoparticles (nZVI) has been extensively applied for reduction of various recalcitrant organic contaminants, but its reactivity usually declines over time due to formation of passive iron oxides. In this study we observed a sustained reactivity of nZVI for dechlorination of carbon tetrachloride (CT) in water during several consecutive reaction cycles. The dechlorination rate constants increased substantially in Cycle 2, then remained at a high level over several consecutive cycles, and ultimately declined in Cycle 7. In the entire process, the solution pH increased only slightly from 7.0 to 7.8, which was different from other unbuffered nZVI reduction systems reported before. Characterization of the particle surface morphology and composition revealed an important role of Fe oxyhydroxides formation in self-buffering the solution pH and sustaining a high nZVI reactivity. Our study provides new knowledge on the nZVI dechlorination process and may offer implications for extending the lifetime of nZVI in wastewater treatment and environmental remediation applications.

1 Introduction

Zero-valent iron nanoparticles (nZVI) has been widely used for environment remediation and contaminant treatment since the late 1990s [1], attributed to its high reactivity for reducing a wide range of contaminants in subsurface environment, such as chlorinated organic compounds [2], nitroaromatic compounds [3], heavy metals [4] and inorganic compounds [5]. Contamination of groundwater aquifers by halogenated organic compounds (e.g., carbon tetrachloride (CT)) presents a severe threat to today's drinking water security. CT is carbinogenic, highly recalcitrant in environment and widely exists in groundwater and soils of many regions [6]. nZVI treatment is an effective and low-cost technology for CT removal. However, a previous study showed that the CT dechlorination kinetics in a pH-buffered solution decreased significantly with the corrison and surface oxidation of nZVI [7]. While, in other studies, the reductive reactivity of aged nZVI (i.e., a layer of iron oxides naturally formed on nZVI surface) in an unbuffered system increased first with the aging time followed by a gradual decrease, due to a combined effect of original iron oxide shells breakdown and new, non-reactive oxides layer formation [8]. Notably, in that study the dechlorination kinetics seemed to remain at a high level for nZVI with the aging time ranging within 2~5 days, but this phenomenon and the pH dynamics were not given attention by the researchers. Interestingly, another study of nitrate reduction showed that the reaction kinetics of nZVI in an unbuffered solution decreased continuously from 9.34 h^{-1} to 1.64 h^{-1} over a 15 h period without a plateau

stage [9]. The solution pH increased rapidly to 9-10 at the reaction beginning and remained almost unchanged throughout the whole reaction process. Based on these findings and the fact that pH could significantly influence dechlorination activity of nZVI [10], it is thus reasonable to expect that the CT dechlorination kinetics,might be highly related to the solution pH and aging of nZVI. However, no direct evidence has been provided so far. In all, it is still unclear.

In this study, we aim to clarify how solution pH would change during CT reduction by nZVI, and whether nZVI, which would become aged with the reaction proceeding, could remain its activity. The dechlorination kinetics of nZVI during several consecutive reaction cycles were investigated. Impacts of pH and ferrous ion on the reaction kinetics were also evaluated. The variations in surface morphologies and compositions of Fe materials were characterized by scanning electron microscopy (SEM), energy dispersive spectrometer (EDS), X-ray diffraction (XRD) and X-ray photoelectron spectroscopy (XPS). An unusual high reactivity of nZVI and a self-buffered solution pH during the decholorination process was demonstrated in this study. The underlying mechanisms were elucidated.

2 Materials and methods

2.1 Materials.

nZVI was synthesized by reducing 0.3 mol/L of $FeSO_4 \cdot 7H_2O$ solution with 0.6 mol/L of $NaBH_4$ solution. The synthesis procedure details and the used chemicals

were provided in the Supporting Information (SI). The synthesized nZVI was washed with deaerated deionized water (DDW) and ethanol followed by filtration. The filtered nZVI particles were vacuum-dried for 12 hours. Ultrapure water (18MΩ•cm, Minipore) was used throughout the experiments.

2.2 CT Reductive Dechlorination by nZVI.

The CT dechlorination experiments were conducted using 250 mL-serum bottles. Prior to the experiment, each bottle was added with 0.05-g nZVI and 100 mL DDW, then immediately bubbled with N_2 (99.9%) for 30 min to ensure anaerobic atmosphere and sealed with Teflon-lined butyl rubber stopper and aluminum crimp cap. To initiate the dechlorination reaction, each bottle was added with 100 μL of CT stock solution (50 mM) prepared in methanol to reach an initial CT concentration of 50 μM. Then, the bottles were put into an orbital shaker at 180 rpm and 30 ± 0.5 °C. After 24 h reaction, each bottle was spiked with another 100 μL of 50 mM CT stock solution to start the next reaction cycle. Seven consecutive dechlorination cycles were performed in this way. The headspace samples of each bottle were collected at given time intervals. To evaluate the possible loss of compounds due to sorption and volatilization, a system without nZVI addition was used as the control. All the experiments were conducted in duplicate.

2.3 Effects of Aqueous Fe(II) and pH.

The effects of aqueous Fe(II) and pH on the reductive dechlorination of CT were investigated by dosing different concentrations of ferrous chloride ($FeCl_2•4H_2O$)

and changing the initial pH, respectively. The original solutions contained 50 μL CT and 0.05 g nZVI. The test solutions with different ferrous concentrations (0.14, 0.529 and 5.29 mmol) were denoted as Fe(II)-1, Fe(II)-2 and Fe(II)-3, respectively, and those with initial pH values of 7 and 10 were marked as pH-7 and pH-10.

2.4 Characterization of Materials.

During nZVI oxidation, changes in morphology and components of Fe oxides/oxyhydroxides on the nZVI surface were identified by SEM, EDS, XRD and XPS. The initial nZVI and the solid samples collected after Cycle 3 (in the high-activity stage) and at the end of the experiment were characterized. More details on instrumentation and sample preparation are provided in the SI.

2.5 Analytical Methods.

Concentrations of CT and its chlorinated products (chloroform (CF) and dichloromethane (DCM)) were determined using headspace analytical technique. Headspace samplings were quantified by an Agilent 6890 gas chromatograph (GC) equipped with an electron capture detector. Methane was measured by a FuLi 9790 GC equipped with a thermal conductivity detector. The concentration of aqueous ferrous was measured using a UV-vis spectrophotometer (Shimadzu UV-1800) at wavelength 510 nm [11]. The solution pH were measured using a pH meter (Mettler Toledo Delta 320). More details on the analytical methods are provided in the SI.

2.6 Statistical analyses of kinetics data.

One-way ANOVA tests available with SPSS18.0 were performed to analyze the variances of the CT dechlorination kinetics in different reaction cycles in this study. A p-value of less than 0.05 indicates a statistically significant difference.

3 Results and discussion

3.1 Pathway of CT reduction by nZVI.

The CT concentration decreased while the content of CF, one of its reduction intermediate, gradually increased during the reaction cycle (Fig. 1) No DCM was detected within the 10 h reaction. In comparison, the nZVI-free control showed no CT degradation. These results indicate that CT was deprived of one chlorine atom by nZVI during the degradation.

Two pathways of CT reductive-transformation have been recognized so far: hydrogenolysis and carbene hydrolysis. Hydrogenolysis can occur through one- or two-electron transfer pathway. One-electron reduction of CT generates a trichloromethyl free radical ($\bullet CCl_3$) that can abstract hydrogen ([H]) to form CF [12]. In the two-electron pathway, the formed $\bullet CCl_3$ is further reduced to obtain a trichloromethyl carbanion ($[:CCl_3]^-$) and form CF [13]. The formation of trichloromethyl carbanion during the two-electron hydrogenolysis can further undergo α-elimination pathway to form dichlorocarbene ($:CCl_2$) via carbene hydrolysis [14]. In this study, generation of DCM was observed only when a completed degradation of CT was achieved. In addition, methane was not detected

120 throughout the experiments (Fig. S1). Perchloroethylene (PCE) was detected during
121 the degradation (Fig. S1), which confirms the presence of trichloromethyl free
122 radical.

123 The kinetics of CT dechlorination and CF formation in the nZVI system can be
124 described by the pseudo-first-order kinetic equation (Eqs.1 and 2).

125 CT degradation:

126 $$[CT]_t = [CT]_0 e^{-k_1 t} \quad (1)$$

127 CF formation:

128 $$[CF]_t = A[CT]_0(1 - e^{-k_1 t}); A = \frac{k_2}{k_1} \quad (2)$$

129 where $[CT]_t$ and $[CF]_t$ are the concentration of CT and CF at sampling time; $[CT]_0$ is
130 the initial CT concentration; k_1 is the observed pseudo-first-order rate constant for
131 CT degradation; k_2 is the rate constant for CF formation, which was calculated using
132 the rate law for parallel first-order formation of reaction products [15]; A is the fraction
133 of CT that is transformed to CF.

134 The fitting curves of CT degradation and CF formation data are also shown in Fig.
135 1. The correlation coefficients were both above 0.992, indicating a good fitting
136 between the experimental data and kinetic values. The estimated reduction rate
137 constants in the first reaction cycle were 0.213 h^{-1} for k_1 and 0.058 h^{-1} for k_2.

138 **3.2 Variation of CT Degradation kinetics.**

139 The CT dechlorination kinetics in several consecutive reaction cycles were
140 investigated and the degradation rate constants were estimated. As shown in Fig. 2,

the dechlorination was significantly accelerated in Cycle 2 (0.501 h^{-1}) compared to the first cycle (0.213 h^{-1}). This acceleration should be attributed to a breakdown of the original iron oxide shell of nZVI which resulted in exposure of the activie Fe(0) to the contaminants [16]. This depasssivation and dissolution of the oxides shell might also explains the distinctly decreased size of the particles after several days of reaction (Fig. 6 and Fig. S4). The rates of hydrogenolysis products (CF and DCM) formation also increased in Cycle 2 correspondingly (Fig. S2).

Interestingly, the CT degradation rate constants showed no significant variation ($p > 0.05$) during Cycles 2-6, but decreased sharply in Cycle 7. A similar variation trend of CT dechlorination kinetics was observed by Sarathy et al [8] who used nZVI of different aging degrees as the reductive agent. In our study, the aging process occurred spontaneously over the reaction process and pH was not controlled, which can better reflect the real process of nZVI corrosion in natural environment.

The reductive chlorination activity of ZVI is governed by the iron surface components and properties. Notably, anaerobic dechlorination (Eq.3) and hydrolysis (Eq.4) are usually accompanied with pH increase and ferrous ions accumulation, which might in turn affect the dechlornation kinetics.

$$Fe^0 + R - Cl + H^+ \rightarrow Fe^{2+} + R - H + Cl^- \quad (3)$$

$$Fe^0 + 2H^+ \rightarrow Fe^{2+} + H_2 \quad (4)$$

3.3 Variations of pH and ferrous ions

To understand the unsual changes of dechlorination kinetics, the variations of pH

and ferrious ions in solution during CT dechlorination were monitored, Fig. 3a shows that the solution pH changed only slightly, suggesting that the system was capable of self-buffering. Meanwhile, the ferrous ions concentration was increased continuously.

It is known that the solution pH could substantially affect the reaction products [18] and species of formed Fe oxides [19]. On the other hand, the ferrous accumulated during the reaction migh play multiple roles in affecting the system reductive activity. For instance, Fe(II) adsorbed on iron oxides could directly reduce a variety of pollutions [20]. However, deposition of some iron oxides on the nZVI surface could also significantly block the electron transfer and decrease the reaction activity. To clarify the inter-correlations between pH and ferrous ion and their roles in dechlorination, the CT degradation under different ferrous concentration and initial pH conditions were tested.

Fig. 4a shows that CT was completely dechlorinated within 3 h for Fe(II)-3, while it took 8 and 10 hours for Fe(II)-2 and Fe(II)-1 respectively, and no CT dechlorination occurred in the nZVI-free system. This result suggests that, although ferrous ions itself cannot reduce CT, the degradation rate was positively correlated to the ferrous concentration when nZVI was present. The final pH of the mixtures were 8.7, 8.2 and 7.7 for Fe(II)-1, Fe(II)-2, Fe(II)-3, respectively (Fig. 4b). The inverse correlation between pH and the added ferrous amount might be due to: (1) ferrous combines with hydroxide ion to form iron oxides and oxyhydroxides,

183 resulting in decreased OH^- concentration; (2) ferrous leads to proton release by
184 substituting the H atom of Fe oxyhydroxides (reactions 5-6) [21].

185 $$\equiv FeOH + Fe^{2+} \leftrightarrow FeOFe(II)^+ + H^+ \quad (5)$$

186 $$\equiv FeOH_2^+ + Fe^{2+} \leftrightarrow FeOFe(II)^+ + 2H^+ \quad (6)$$

187 According to the above mechanism, the continously-generated ferrous during the
188 dechlorination might serve as an effective buffer to neutralize the alkali produced
189 from nZVI corrosion, thereby sustaining a stable pH in the entire reaction process
190 (Fig. 3). This self-buffered pH due to formation of iron oxohydroxides might also be
191 one important reason for the sustained high dechlorination activity of nZVI over the
192 consecutive reaction cycles. As evidenced in Fig. 5, significantly higher CT
193 dechlorination rate was obtained in neutral pH system (0.211 h^{-1} for pH-7 versus
194 0.110 h^{-1} for pH-10). Under alkaline condition, the dechlorination thermodynamics
195 becomes less favorable and meanwhile a thick iron oxides coat would be built on the
196 particle surface to severely block the electron transfer from the iron core [22,23,9].

197 **3.4 Characterization of nZVI and formed ion oxides.**

198 Characterizaton of the solid-phase samples collected at different reaction stages
199 confirms the formation of iron oxohydroxides during the consecutive dechlorination
200 cycles.

201 SEM examination revealed that the initial nZVI contained abundant nanosphere
202 clusters (Fig. 6a), which was typical of nZVI particles. The diameters of the
203 nanospheres were in the range of 50-200 nm. The EDS result clearly showed the

elemental mapping of Fe and O in the nanonecklace structure (Fig. 6b), implying that the nZVI used in our study was slightly oxidized. This happens frequently during the synthesis, drying, storage and application processes, where nZVI with high activity could be easily oxidized to form a thin layer of iron oxides on the surface when exposed to the atmosphere or water. However, the morphology and components of nZVI changed significantly after three dechlorination cycles. Both the number and size of nanospheres decreased, while large amount of platy Fe oxide minerals with bulk and laminated structures were formed (Fig. 6c, Fig. S4b). Notably, the particle area and the bulk mineral area showed no significant difference in the iron and oxygen contents, indicating a similar composition of the iron hydroxides on the particle surface in the precipitate (Fig. S4b). In addition, the EDS data showed that the oxygen content increased from 6% in the initial nZVI to 25% after Cycle 3 (Fig. 6b, 6d). These results confirm that Fe oxohydroxides were formed accompanied with the continous ZVI corrosion. These newly-formed porous Fe oxides posed insignficantly impacts on the corrosion of the ZVI particles and might even directly contributed to CT dechlorination by utilizing the adsorbed Fe(II) [17]. At the end of the experiment, more bulk and dense-structured iron precipitates were observed, which might to some extent hamper the electron transfer from the buried particles ZVI particles (Fig. S3, S4).

The variations of nZVI composition during reaction were validated by XRD and XPS. Pure Fe, with the XRD peaks of 44.9 and 65.0°, was identified for the initial

nZVI Fe (Fig. 7a). However, this XRD signal was weak, indicating a relatively low crystallinity. Meanwhile, no distinct peaks of iron oxides were observed, implying a small amount or poor crystallinity of the oxides shell [24]. The XPS spectra revealed that only elements Fe, O, and C existed in the original nZVI (Fig. S5a). The C1s peak at 284.8 eV should be attributed to the adventitious carbon (Fig. S5b). For the original nZVI, two narrow distinct peaks of similar intensity, 709.89 eV and 710.95 eV, separated by about 1 eV were detected (Fig. 8a). The peak positions were consistent with the literature values of 709.7 and 710.8 eV assigned to Fe2p 3/2 for α-Fe_2O_3. Two other prominent peaks also occurred, which are ascribed to a satellite band at 719.30 about 8 eV above the Fe (2p 3/2) line and the shoulder peak at 724.50 eV in the high resolution spectra [25]. These data confirm that the oxide shells of the Fe(0) core were Fe_2O_3. Besides the predominant peaks of Fe in Fe_2O_3, a peak at a low binding energy of 706.9 eV, attributed to Fe2p 1/2 in pure Fe, was also detected, indicating that the thickness of the Fe_2O_3 shell should be less than 10 nm since the XPS could only detect the photoelectrons from the outer surface of 10 nm.

After three CT dechlorination cycles, obvious peaks of iron oxides and oxyhydroxides occurred while the peaks of Fe(0) remained, suggesting a significant change of the iron oxides composition. It has been reported that certain iron oxides/oxyhydroxides, such as green rust, ferrihydrite and magnetite, could promote the reductive transformation of contaminants [26, 27]. The evolution of surface chemical compositions of nZVI during the reaction was further convinced by XPS

246 analysis. The peaks of pure iron disappeared after Cycle 3 (Fig. 8c), likely due to
247 decreased Fe(0) content and the inclusion of Fe particles within the Fe oxides
248 matrixes.. The high-resolution XPS spectra of O 1s could be fitted by two peaks at
249 binding energies of about 529.77 and 531.02 eV, respectively (Fig. 8b and 8d). The
250 dominant peak at 529.77 eV is assigned to the lattice oxygen of Fe (Fe_2O_3) , while
251 the other O1s peaks at around 531.02 eV is ascribed to adsorbed hydroxyl (Fe-OH_{ad}),
252 lattice hydroxyl (Fe-$OH_{lattice}$) and water (H_2O) [28], which we denoted as bonded-OH
253 here. It is obvious that the bounded-OH content increased during the dechlorination,
254 which is in accordance with the strengthened signals of Fe oxyhydroxides detected
255 by XRD (Fig. 7b).

256 With the further proceeding of dechlorination reactions, other ion oxides such as
257 magnetite, hematite and goethite also occurred at the end of the experiments, as
258 demonstrated by the XRD data (Fig. S6). The formation of these iron oxides have
259 been reported to suppress the reduction of chlorinated organics [29]. Therefore, these
260 inactive iron oxides might form a matrix of dense structure and block the electron
261 transfer from the buried nZVI particles. In addition, the amount of nZVI might
262 become limiting at this stage due to continous consumption. Thus, the decreased
263 nZVI amount might also account for the dereased dechlorination kinetics at Cycle 7.

264 **3.5 Mechanisms of sustained high dechlorination activity of nZVI.**

265 Based on the above analysis, we propose the following mechanisms of the
266 sustained high dechlorination activity of nZVI (Fig. 9). In the intial reaction (Cycle

1), the Fe(0) core of nZVI was mainly responsible for CT reduction. However, the electrons from Fe(0) core have to pass through an iron oxide shell. This oxide shell increased the electron transfer resistence and resulted in relatively low dechlorination kinetics. With the proceeding of reaction, this oxide shell is broken down and meanwhile some loose-structured more permeable active oxides precipitates are formed and deposited both on the particle surface and in the bulk solution (Fig. S4). As a consequence, more Fe(0) are exposed and become available for direct CT reduction. In the meantime, the newly-formed Fe oxohydroxides don't significantly block the electron flow from inner Fe particles, and may even directly participate in the dechlorination by utilizing the active adsorbed Fe(II) [30,31]. Another important factor is that the formation of Fe oxohydroxides resulted in a self-buffering of the solution pH. On one hand, the corrosion of nZVI and reductive dechlorination results in more ferrous and increased pH (Eq. 3 and 4). On the other, the generated ferrous continuously consume alkali by directly combining with OH^- to form oxyhydroxides and further complexing with the oxyhydroxides to release H^+. Therefore, all the above factors together result in a stable pH and sustained dechlorination kinetics over several reaction cycles. Notably, the amount and size of Fe(0) particles would decrease over due to the continuous consumption (Fig. S4). In the meantime, the amount, composition and structure of the Fe oxohydroxides would gradually change, resulting in less active oxohydroxides and higher electron transfer resistance from the inner ZVI. All these two factors might eventually lead to

288 decreased dechlorination kinetics by nZVI during long-time reaction.

289

290 **4 Conclusions**

291 The present study demonstrates that nZVI can be efficiently used for the reductive
292 dechlorination of CT with a pH self-buffering ability and sustained high activity. A
293 breakdown of the original oxide shell and meanwhile the generation of a more active,
294 porous oxohydroxides contributed to the significantly acccelerated dechlorination
295 compared to the initial nZVI. The formation of Fe oxohydroxides was also an
296 important reason of the pH self-buffering in our system. However, the
297 dechlorination kinetics eventually declined after a long-time reaction due to
298 decreased amount of nZVI particles and changes of the Fe oxohydroxides
299 composition and structure. These findings imply a high potential to maintain a high
300 activity of nZVI in natural environment by controlling appropriate pH and ferrous
301 level, and may provide implications for in-situ remediation of chlorinated
302 contaminants and other oxidative species in subsurface environment.

303

304 **Acknowledgements**

305 The authors wish to thank the National Nature Science Foundation of China
306 (51278479), the National 863 Project (2011AA060901), the Hundred-Talent
307 Program of Chinese Academy of Sciences, the Program for Changjiang Scholars and
308 Innovative Research Team in University, the Fundamental Research Funds for the

Central Universities (wk2060190040)，the Collaborative Innovation Center of Suzhou Nano Science and Technology, and the Hong Kong University Grants Committee (AoE/P-03-08) for the financial support of this work.

References

1. D. O'Carroll, B. Sleep, M. Krol, H. Boparai and C. Kocur, *Adv. Wat. Resour.*, 2013, **51**, 104-122.
2. M. Zhang, F. He, D. Zhao and X. Hao, *Water Res.*, 2011, **45**, 2401-2414.
3. Y. Mu, H. Q. Yu, J. C. Zheng, S. J. Zhang and G. P. Sheng, *Chemosphere*, 2004, **54**, 789-794.
4. L. N. Shi, X. Zhang and Z. L. Chen, *Water Res.*, 2011, **45**, 886-92.
5. S. R. Kanel, B. Manning, L. Charlet and H. Choi, *Environ. Sci. Technol.*, 2005, **39**, 1291-1298.
6. C. Penny, S. Vuilleumier and F. Bringel, *FEMS Microbiol. Ecol.*, 2010, **74**, 257-275.
7. S. Bae and W. Lee, *Environ. Sci. Technol.*, 2014, **48**, 2368-76.
8. V. Sarathy, P. G. Tratnyek, J. T. Nurmi, D. R. Baer, J. E. Amonette, C. L. Chun, R. L. Penn and E. J. Reardon, *J. Phys. Chem. C*, 2008, **112**, 2286-2293.
9. K. Sohn, S. W. Kang, S. Ahn, M. Woo and S.-K. Yang, *Environ. Sci. Technol.*, 2006, **40**, 5514-5519.
10. Y. Liu and G. V. Lowry, *Environ. Sci. Technol.*, 2006, **40**, 6085-6090.

11. Z. Ai, Z. Gao, L. Zhang, W. He and J. J. Yin, *Environ. Sci. Technol.*, 2013, **47**, 5344-52.

12. H. J. Ahr, L. J. King, W. Nastainczyk and V. Ullrich, *Biochem. Pharmacol.*, 1980, **29**, 2855-2861.

13. J. Hine, R. C. Peek Jr and B. D. Oakes, *J. Am. Chem. Soc.*, 1954, **76**, 827-829.

14. M. L. McCormick and P. Adriaens, *Environ. Sci. Technol.*, 2004, **38**, 1045-1053.

15. Y. T. Lin and C. Liang, *Environ. Sci. Technol.*, 2013, **47**, 3299-3307.

16. J. T. Nurmi, P. G. Tratnyek, V. Sarathy, D. R. Baer, J. E. Amonette, K. Pecher, C. Wang, J. C. Linehan, D. W. Matson and R. L. Penn, *Environ. Sci. Technol.*, 2005, **39**, 1221-1230.

17. J. Filip, F. Karlický, Z. Marušák, P. Lazar, M. Černík, M. Otyepka and R. Zbořil, *The Journal of Physical Chemistry C*, 2014, **118**, 13817-13825.

18. K. M. Danielsen and K. F. Hayes, *Environ. Sci. Technol.*, 2004, **38**, 4745-4752.

19. H. Y. Jeong, K. Anantharaman, S. P. Hyun, M. Son and K. F. Hayes, *Water Res.*, 2013, **47**, 6639-49.

20. J. E. Amonette, D. J. Workman, D. W. Kennedy, J. S. Fruchter and Y. A. Gorby, *Environ. Sci. Technol.*, 2000, **34**, 4606-4613.

21. T. Liu, X. Li and T. D. Waite, *Environ. Sci. Technol.*, 2013, **47**, 13712-20.

22. N. Sato, T. Noda and K. Kudo, *Electrochim. Acta*, 1974, **19**, 471-475.

23. T. L. Johnson, W. Fish, Y. A. Gorby and P. G. Tratnyek, *J. Contam. Hydrol.*, 1998, **29**, 379-398.

24. L. Lu, Z. Ai, J. Li, Z. Zheng, Q. Li and L. Zhang, *Cryst. Growth Des.*, 2007, **7**, 459-464.

25. N. McIntyre and D. Zetaruk, *Anal. Chem.*, 1977, **49**, 1521-1529.

26. M. Erbs, H. C. Bruun Hansen and C. E. Olsen, *Environ. Sci. Technol.*, 1999, **33**, 307-311.

27. R. A. Doong, C. C. Lee and C. M. Lien, *Chemosphere*, 2014, **97**, 54-63.

28. X. Zhou, J. Lan, G. Liu, K. Deng, Y. Yang, G. Nie, J. Yu and L. Zhi, *Angew. Chem. Int. Ed. Engl.*, 2012, **51**, 178-82.

29. J. Farrell, M. Kason, N. Melitas and T. Li, *Environ. Sci. Technol.*, 2000, **34**, 514-521.

30. J.-L. Chen, S. R. Al-Abed, J. A. Ryan and Z. Li, *J. Hazard. Mater.*, 2001, **83**, 243-254.

31. M. Elsner, R. P. Schwarzenbach and S. B. Haderlein, *Environ. Sci. Technol.*, 2004, **38**, 799-807.

Figure captions:

Fig. 1. Reductive dechlorination of CT by nZVI for the first cycle. Lines show the fits of the data to the model of CT degradation and CF formation. Error bars are the ranges of duplicate samples.

Fig. 2. Reductive dechlorination kinetics of CT by nZVI for seven cycles. Error bars are the ranges of duplicate samples.

Fig. 3. The variation of pH and ferrous during the CT dechlorination by nZVI.

Fig. 4. (a) CT reductive dechlorination by nZVI with different addition of ferrous and (b) the final pH. Error bars are the ranges of duplicate samples.

Fig. 5. (a) Profiles of CT concentration as a function of reaction time during the anaerobic dechlorination by nZVI with different initial pH. Error bars are the ranges of duplicate samples. (b) Degradation kinetics of CT with different initial pH (7 and 10).

Fig. 6. (a) SEM image and (b) EDS analysis of nZVI; (c) SEM image and (d) EDS analysis of Aged-nZVI after Cycle 3.

Fig. 7. XRD analysis of (a) nZVI and (b) Aged-nZVI after Cycle 3.

Fig. 8. (a) XPS-nZVI high resolution spectra of Fe 2p; (b) XPS-nZVI high

resolution spectra of O1s; (c) XPS-Aged-nZVI (after Cycle 3) high resolution spectra of Fe 2p; (d) XPS-Aged-nZVI (after Cycle 3) high resolution spectra of O1s.

Fig. 9. Hypothesized mechanism of sustained CT dechlorination activity of nZVI over consecutive reaction cycles.

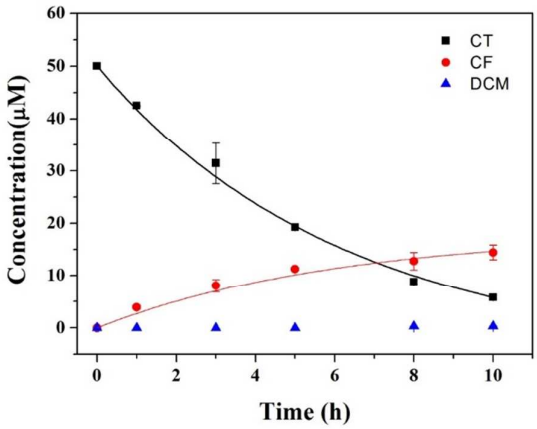

Fig. 1. Reductive degradation of CT by nZVI for the first cycle. Lines show the fits of the data to the model of CT degradation and CF formation. Error bars are the ranges of duplicate samples.

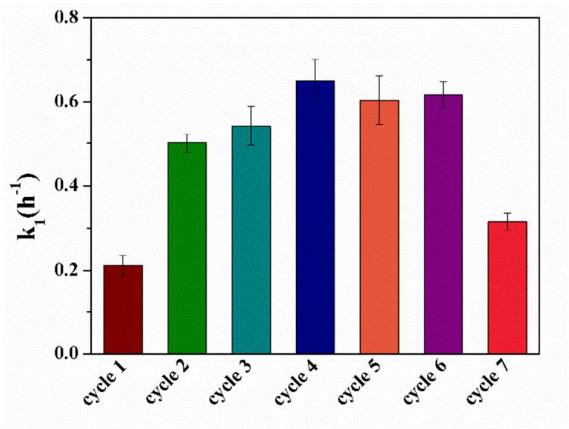

Fig. 2. Reductive dechlorination kinetics of CT by nZVI. Error bars are the ranges of duplicate samples.

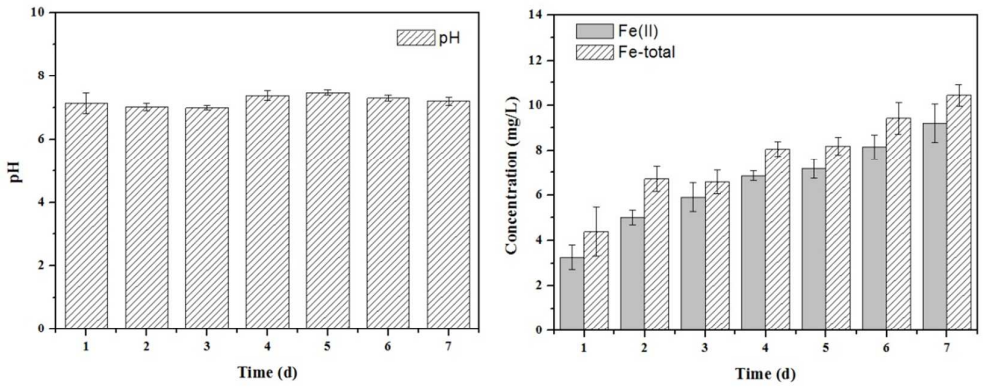

Fig. 3. The variation of pH and ferrous during the CT dechlorination by nZVI.

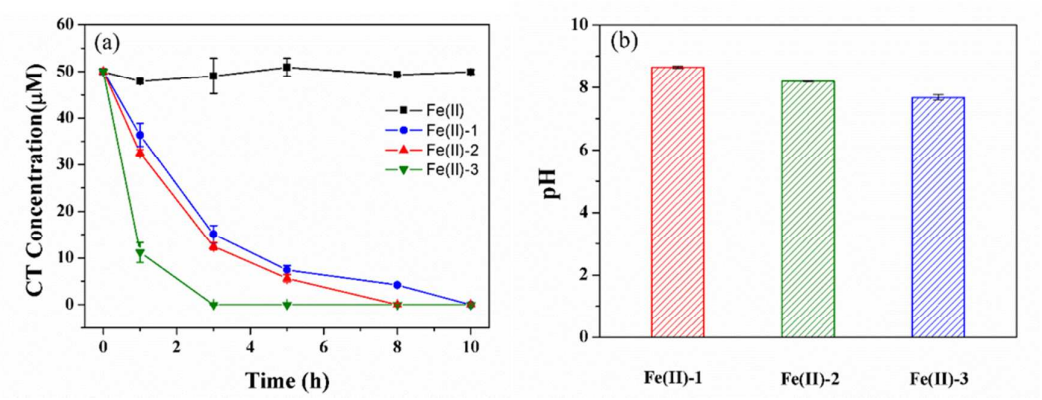

Fig. 4. (a) CT reductive dechlorination by nZVI with different addition of ferrous and (b) the final pH. Error bars are the ranges of duplicate samples.

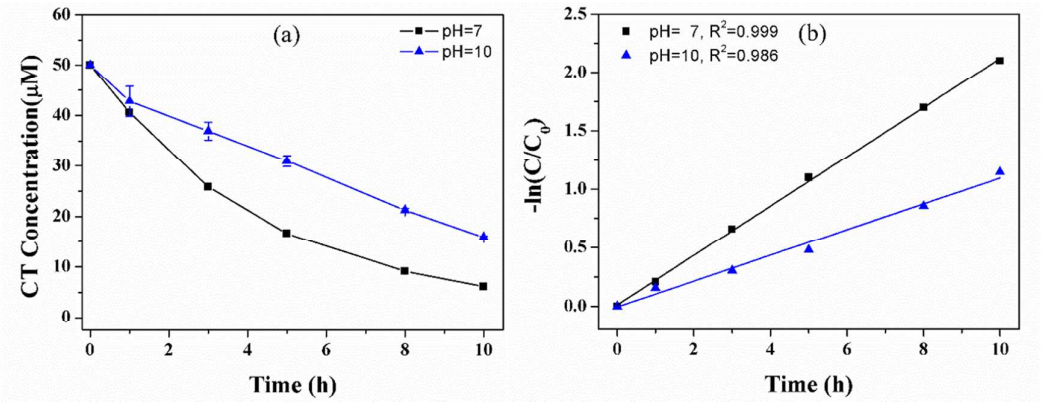

Fig. 5. (a) Profiles of CT concentration as a function of reaction time during the anaerobic dechlorination by nZVI with different initial pH. Error bars are the ranges of duplicate samples. (b) Degradation kinetics of CT with different initial pH (7 and 10).

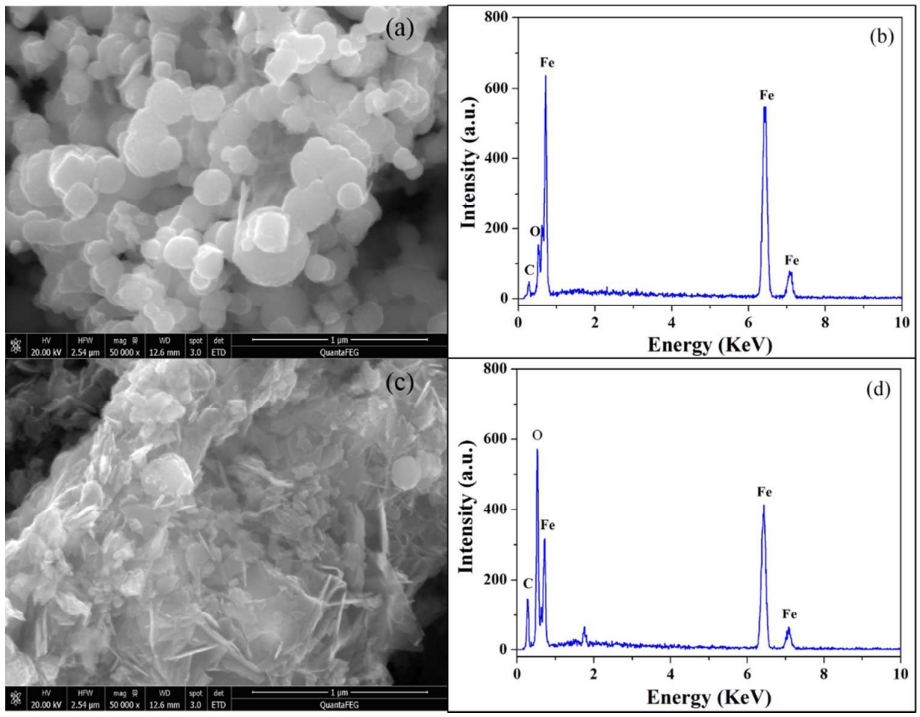

Fig. 6. (a) SEM image and (b) EDS analysis of initial nZVI; (c) SEM image and (d) EDS analysis of nZVI after Cycle 3.

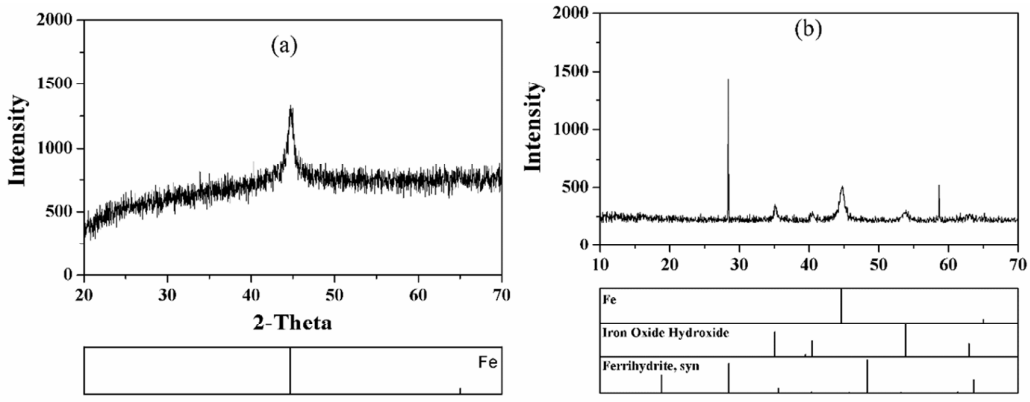

Fig. 7. XRD analysis of (a) initial nZVI and (b) after Cycle 3.

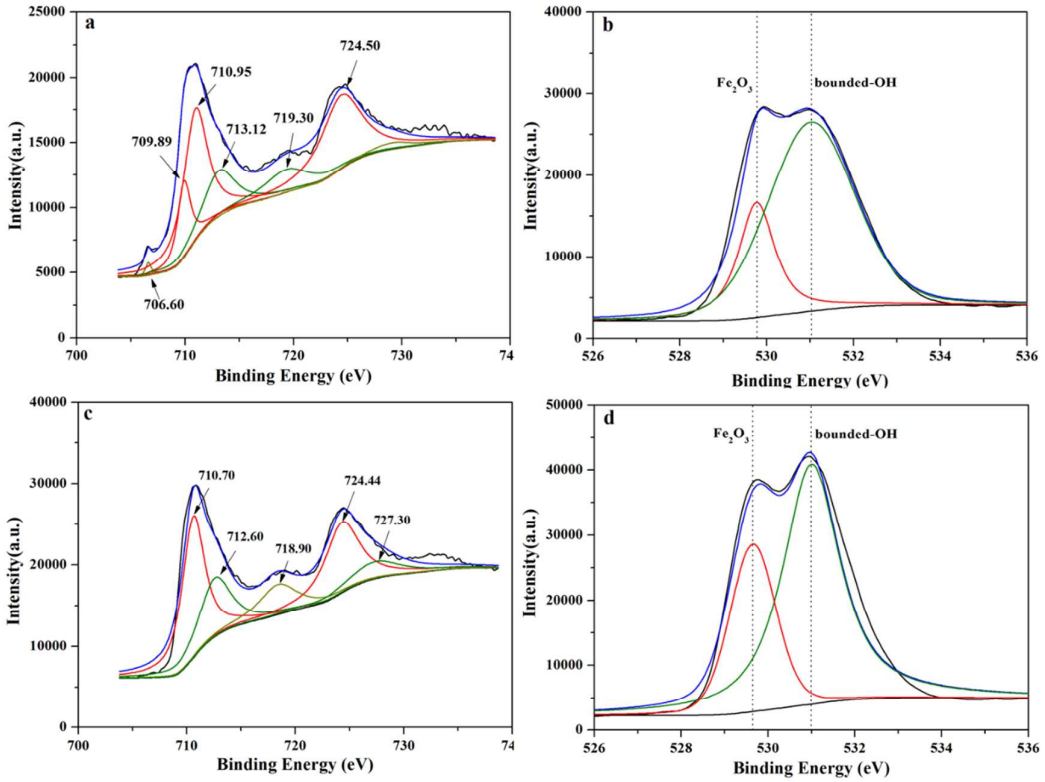

Fig. 8. High resolution XPS spectra of (a) Fe 2p and (b) O1s for initial nZVI; High resolution XPS spectra of (c) Fe 2p and (d) O1s for nZVI after Cycle 3.

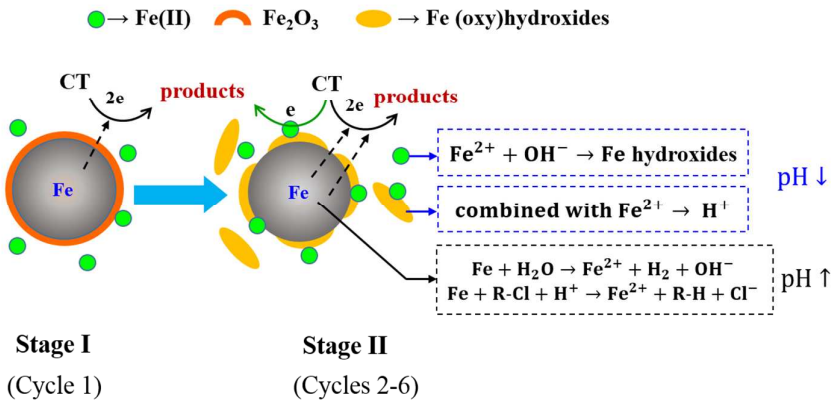

Fig. 9. Hypothesized mechanism of CT dechlorination by nZVI.